Supporting Information

Solvothermal synthesis of 3D rod-like Fe-Al bimetallic metal-organic framework for efficient fluoride adsorption and photodegradation of water-soluble carcinogenic dyes

Arnab Mukherjee[1], Prasanta Dhak[2], Debasis Dhak[1]*

[1] Nanomaterials Research Lab, Department of Chemistry, Sidho-Kanho-Birsha University, Purulia-723104, India

[2] Department of Chemistry, Techno India University, Kolkata – 700091, India

*Corresponding author, E-mail: debasis.chem@skbu.ac.in, debasisdhak@yahoo.co.in

The degree of the use of water-soluble dyes (e.g. methylene blue) in different industrial applications [1], followed by their continuous discharge of contaminated waste-water into the water-bodies causes serious issues for both the environment (damaging the aquatic biota) and human beings (e.g. heart disease, lung and urinary bladder cancer, chromosomal fractures, mutagenesis, and respiratory toxicity, etc.) also [2]. Besides fluoride (F^-) is one such toxic element polluting the groundwater through natural sources as well as the from the industry [3] and chronic intake of fluorinated water beyond the permissible limit (>1.5 ppm according to WHO) causes dental/skeletal fluorosis [4]. The natural sources of F^- are geological processes e.g. the rock and water interaction, geothermal spring, volcanic and tectonic processes, weathering, etc. [5] are the major pathways for F^- contamination and some man-made or anthropogenic sources are phosphate fertilizers, rodenticide, fumigants, herbicides, insecticides containing F^- as an impurity and from steel, aluminum, glass and tile industries [6], etc. Thus, it is needful to eliminate F^- and the colored wastewater staffs for the sack of the environment using some eco-friendly method.

Analytical measurements

The thermogravimetric analysis (TGA) (Perkin Elmer STA 6000) was done from ambient temperature to 800°C at a heating rate of 10°C/min using α-alumina as a standard in the N_2 atmosphere. For the solvothermal synthesis, a Hydrothermal Oven (EYELA, Ser. No. 11614615) has been used. The nanopowders were characterized by X-ray diffraction (Model SmartLab SE, Rigaku, Japan); CuKα (λ = 1.5406 Å) was used at a scanning speed of 2^o 2θ/min and indexed with standard JCPDS files. The optical density (UV-vis DRS), dye concentration, and fluoride concentration were done by the UV-vis spectrophotometer (PerkinElmer, LAMBDA35). Fourier transform-infrared spectroscopy (FTIR) was documented in the range of 4000-500 cm^{-1} using the KBr pellet method using the Perkin Elmer Spectrum model no. L1600300. A scanning electron microscope (Model JSM 5800 Jeol, Tokyo, Japan) was used to observe the surface morphology and other topographic information. The specific surface area was determined by the N_2 adsorption/desorption method at a liquid N_2 temperature of 77.350 K using NOVA touch 4LX (F/W ver. 1.05, Serial# 17018101901), Quanta chrome, USA. Raman spectra were done using Witec alpha300R using a laser wavelength of 532 nm and a spot size of 100 nm. Electron Spin Resonance (ESR) was done using Electron Spin Resonance (ESR) Spectrometer JEOL, Model: JES-FA200 for room temperature X-band analysis. The X-ray photoelectron spectroscopy (XPS) analysis has been done using JPS-9030 photoelectron spectrometer, JEOL, Tokyo, Japan with a monochromatic Al Kα X-ray source. The concentration of fluoride, pH studies, and other physical parameters was done using Thermo Scientific (Orion Versa star Pro) Advance Electrochemistry Meter (Software Revision: r4.06, serial number: V11855). The ξ-potential investigation was done using Malvern Zetasizer Nano ZS90 (United Kingdom). The PL emission spectra was recorded using Perkin Elmer Fluorescence Spectrometer LS 55 (United Kingdom). The high-performance liquid chromatography (HPLC), of MB and its photodegraded products, were done using Thermo Scientific UHPLC 3000 with Thermo Scientific Hypersil GOLD aQ, Part No. 25303-154630 (150 × 4.6 mm) column with 3 μ particle size, mobile phase consisted of acetonitrile/water (70:30) for RhB and methanol/water (80:20), and the flow rate was set 1.0 mL/min. Approximately 25 μL volume of samples were injected into the column and the effluent was monitored at 550 nm for RhB and 663 nm for MB respectively.

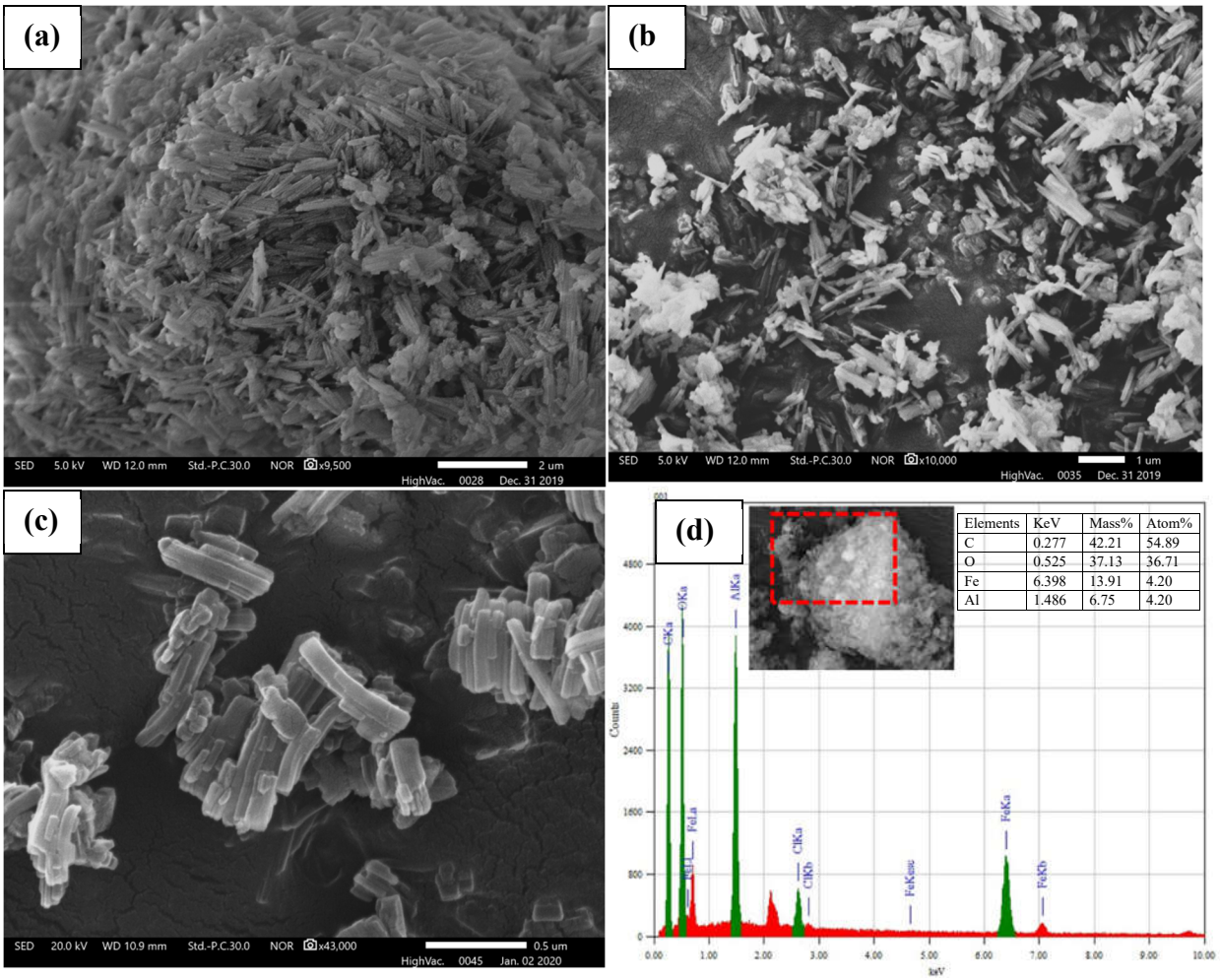

Fig.S1. FESEM images of the bi-metallic MOF synthesized in different temperatures for the 70 h (a) 373K, (b) 423K, and (c) 473K and (d) SAEDS analysis of (inset-quantitative analysis) Fe-Al BDC prepared at 473K for 70h respectively.

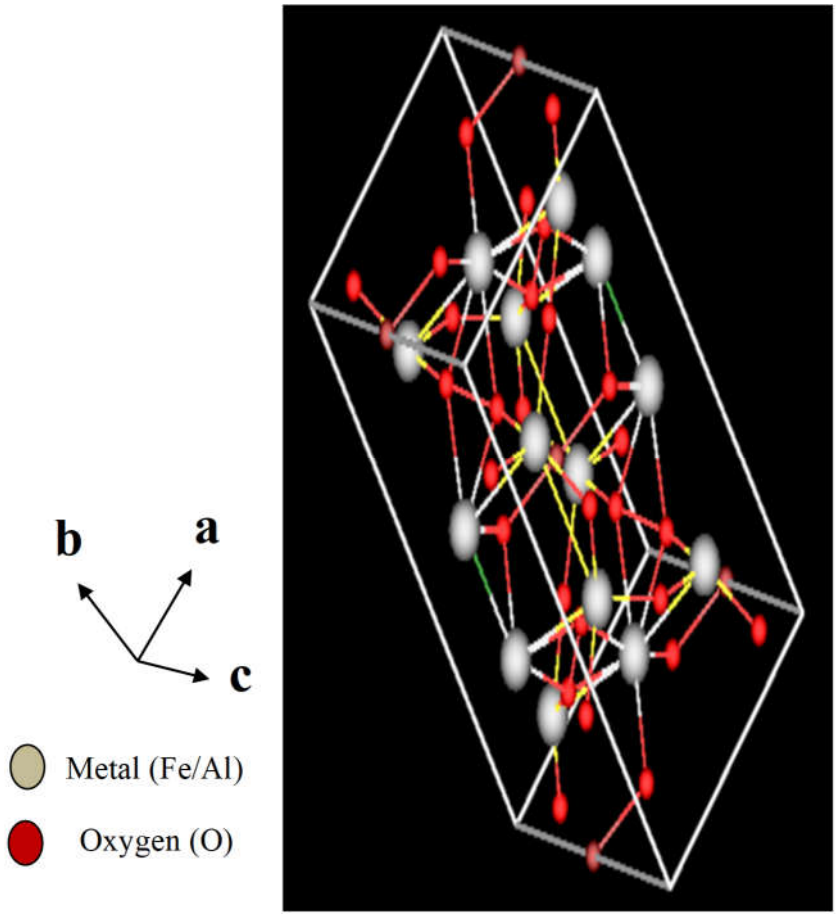

Fig.S2. The structure of Fe-Al BDC was obtained from the PXRD analysis prepared at 473K for 70h.

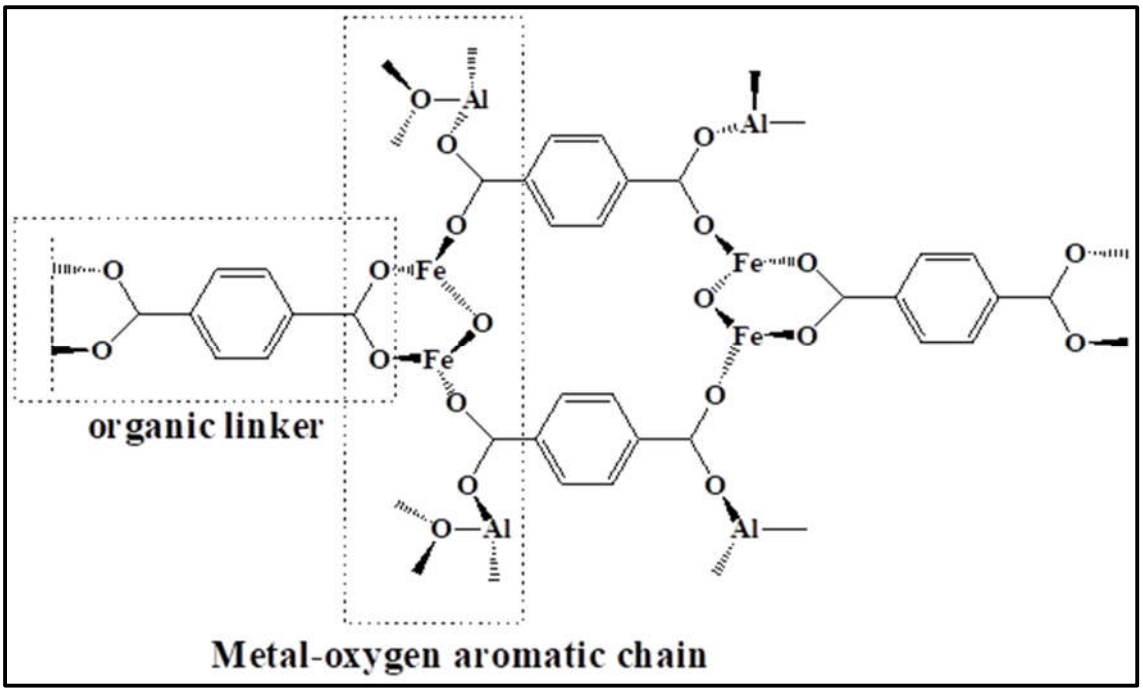

Fig.S3. The proposed chemical structure of Fe-Al BDC was obtained from the PXRD analysis prepared at 473K for 70h.

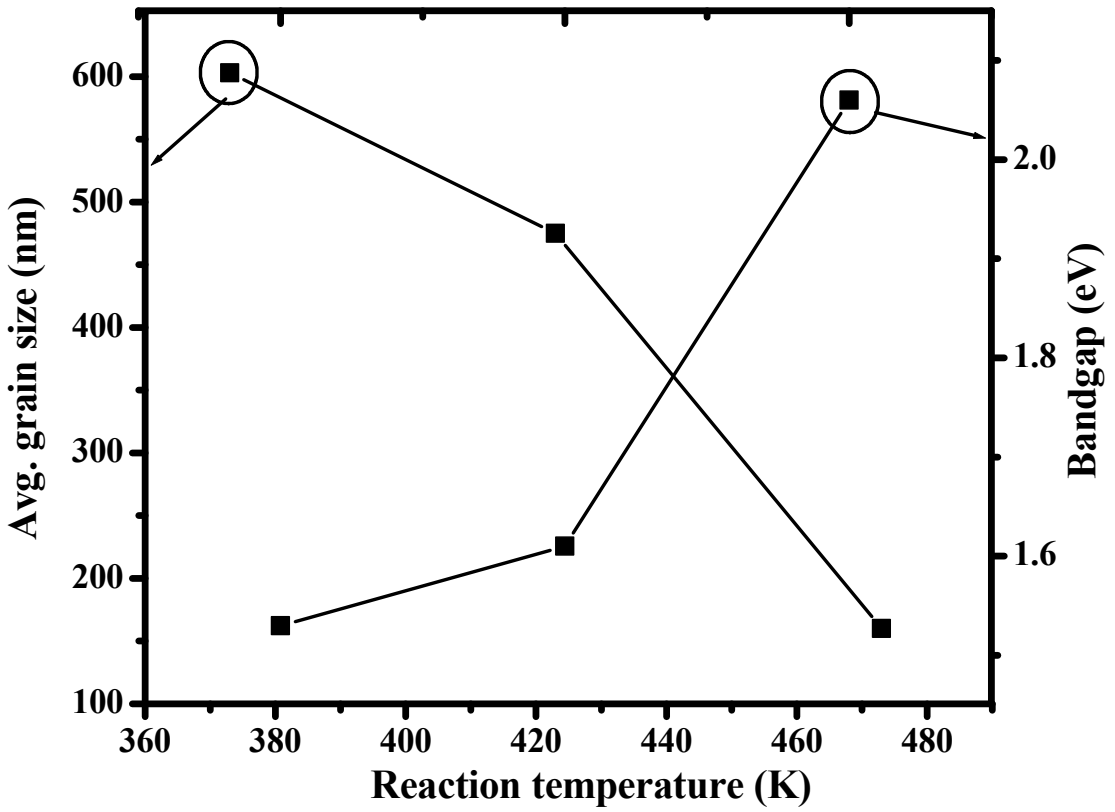

Fig.S4. Variation of average grain size (nm) revealed from FESEM studies and bandgap (eV) calculated using Tauc's method of the same concentration of the precursor heated at 473K for different reaction times (24h, 48h, and 70h).

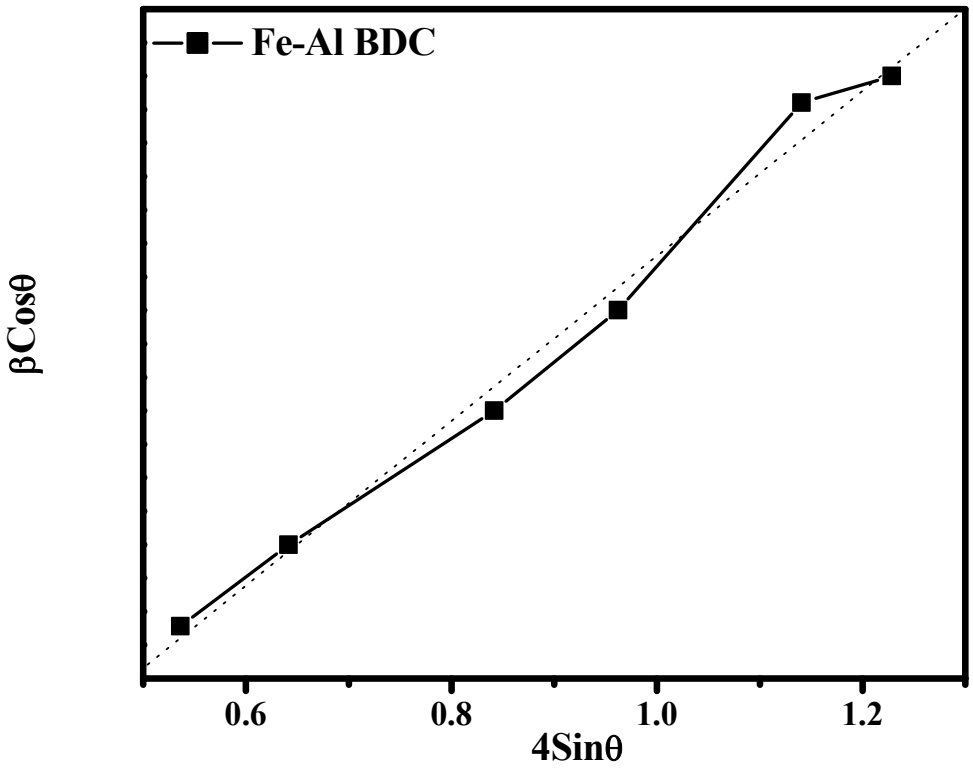

Fig.S5. Williamsone-Hall (W-H) plot of Fe-Al BDC prepared at 473K for 70h.

Table S1. PXRD analysis results of Fe-Al BDC using Scherrer's method, Williamson-Hall method, and ICP analytical data prepared at 473K for 70h.

Sample	Unit cell parameters (Å)	Crystallite size (nm)		Avg. cell volume ($Å^3$)	Strain (ε)	SF*	δ# (line/m^2)
		Scherrer's method	W-H plot				
Fe-Al BDC	a = 11.48 b = 10.45 c = 7.00	26.85	28.28	840	0.00246	0.4857	0.00125
ICP analytical data							
Sample	Fe (wt%)			Al (wt%)			
Fe-Al BDC	13.90±0.05			6.75±0.05			

* SF=stacking fault, #δ= distortion density

Relation between the particle size and surface area

The relation between the particle size (obtained by the PXRD analysis) and the surface area has been developed by André et al. [7]. In this work, the optimum condition for the phase pure bimetallic MOF Fe-Al BDC has been developed using the solvothermal method keeping a constant reaction time (70h) and varying the reaction temperature (373K, 423K, and 473K). The development of products has been confirmed by the PXRD and FESEM analyses. FESEM investigations showed that with the increase in reaction temperature the formation of the 3D rod-like structure has been developed as shown in Fig.S1a-c and the synthesized particles at 473K for 70h is phase pure with a perfect 3D rod-like geometry. The PXRD results were matched with the standard JCPDS file no. 84-2232 and Fe-Al BDC (473K, 70h) was a monoclinic unit cell structure with space group (S.G) C2/c(15). For the monoclinic parallelepiped a≠b≠c and using the André relation

$a = lb$ and $c = mb$, where l and m are the relation constants, thus the materials constant could be evaluated as, $\beta = 1 + l^{-1} + m^{-1}$ [7]. The l, and m values along with the particle size and the surface area data are given in Table S2.

Table S2. Particle size, BET surface area, relation constants, and representative particle radius (R_{REP}^{-1}) of the synthesized bimetallic MOF at different temperatures (373K, 423K, and 473K) for 70h.

Material	Particle size (nm)	S_{BET} (m^2/g)	l	m	β	R_{REP}^{-1}
373	170.23	0.523	1.2377	0.5276	3.7033	10.23
423	80.33	29.602	1.9365	0.6259	1.5637	16.33
473	26.85	120.255	1.6385	0.6704	1.2807	30.23

Calculating the β values the André particle edges were calculated to evaluate the R_{REP} i.e., the representative particle radius using the Eq. S1.

$$R_{REP}^{-1} = \frac{2(d_2^3 - d_1^3)}{3(d_2^3 - d_1^3)} \ldots\ldots\ldots \text{(S1)}$$

Where d_2 and d_1 are the lower and upper edge lengths respectively.

In Fig.S6, the BET surface area has been plotted against the R_{REP}^{-1} and a linear plot ($R^2 = 0.997$) has been obtained which firmly established that with decreasing the particle size the surface area is increased.

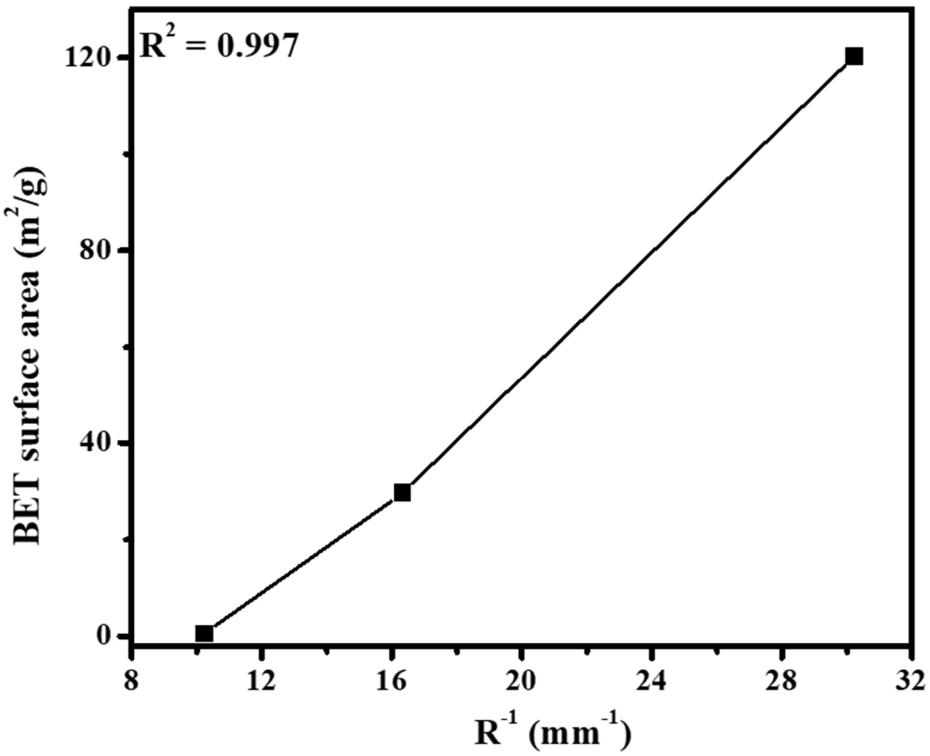

Fig.S6. The specific surface area of bimetallic MOFs prepared at different temperatures for 70h as a function of the inverse of the representative particle radius (R_{REP}^{-1}).

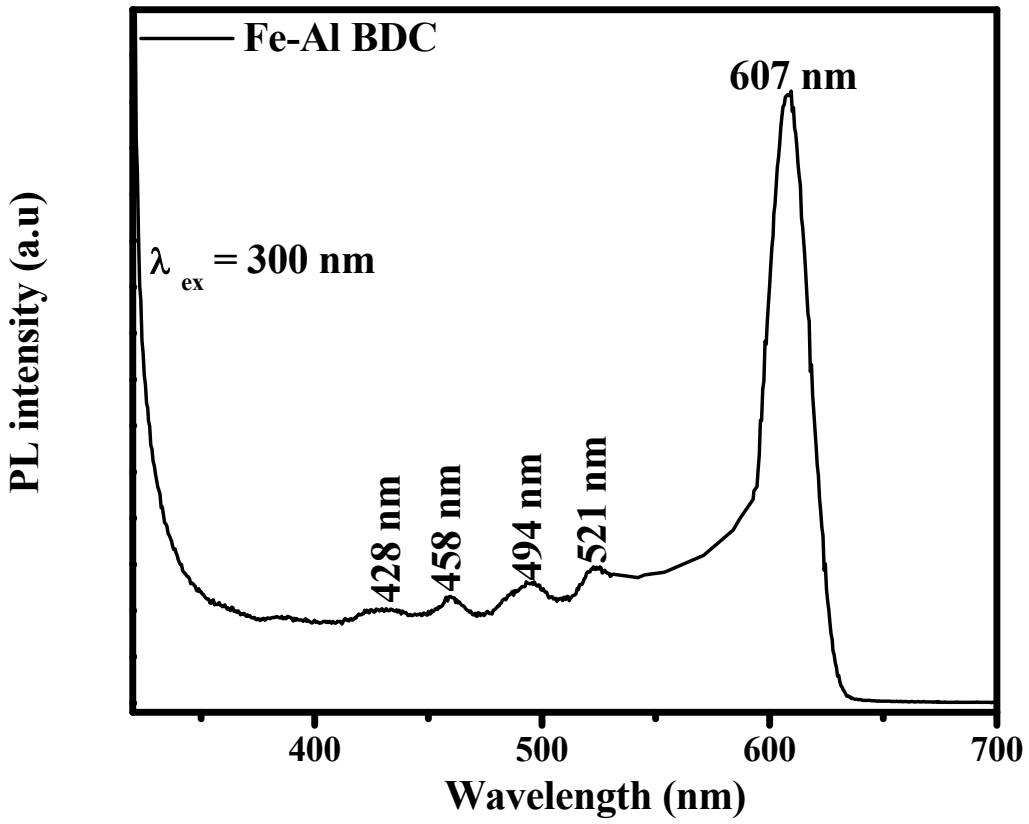

Fig.S7. Photoluminescence (PL) emission spectrum of Fe-Al BDC excited at 300 nm prepared at 473K for 70h.

Table S3. Removal of F^- and pseudo-2nd-order kinetic data using Fe-Al BDC prepared at 473K for 70h at 30°C, pH 7.

Serial no.	Initial F^- conc. (ppm)	Adsorbent dose (g/100 mL)	Time (min)	Removal	k_2 (g min/mg) ($\times 10^{-1}$)	R^2
1.	3	0.05	15	82.00	0.103	0.994
2.			30	74.00		
3.			45	79.66		
4.			60	85.33		
5.		0.10	15	86.00	0.104	0.999
6.			30	83.66		
7.			45	86.00		
8.			60	86.33		
9.		0.15	15	87.66	0.104	0.999
10.			30	87.33		
11.			45	84.66		
12.			60	85.33		
13.	5	0.05	15	90.20	0.133	0.999
14.			30	89.60		
15.			45	90.20		
16.			60	90.60		
17.		0.10	15	91.40	0.160	0.999
18.			30	90.20		
19.			45	90.20		
20.			60	92.20		
21.		0.15	15	90.80	0.178	0.999
22.			30	90.80		
23.			45	90.80		
24.			60	90.80		
25.	10	0.05	15	87.00	0.836	0.999

26.			30	84.00		
27.			45	84.00		
28.			60	84.00		
29.		0.10	15	91.60	1.076	0.999
30.			30	91.80		
31.			45	95.60		
32.			60	95.40		
33.		0.15	15	88.00	0.991	0.999
34.			30	88.00		
35.			45	89.00		
36.			60	88.00		

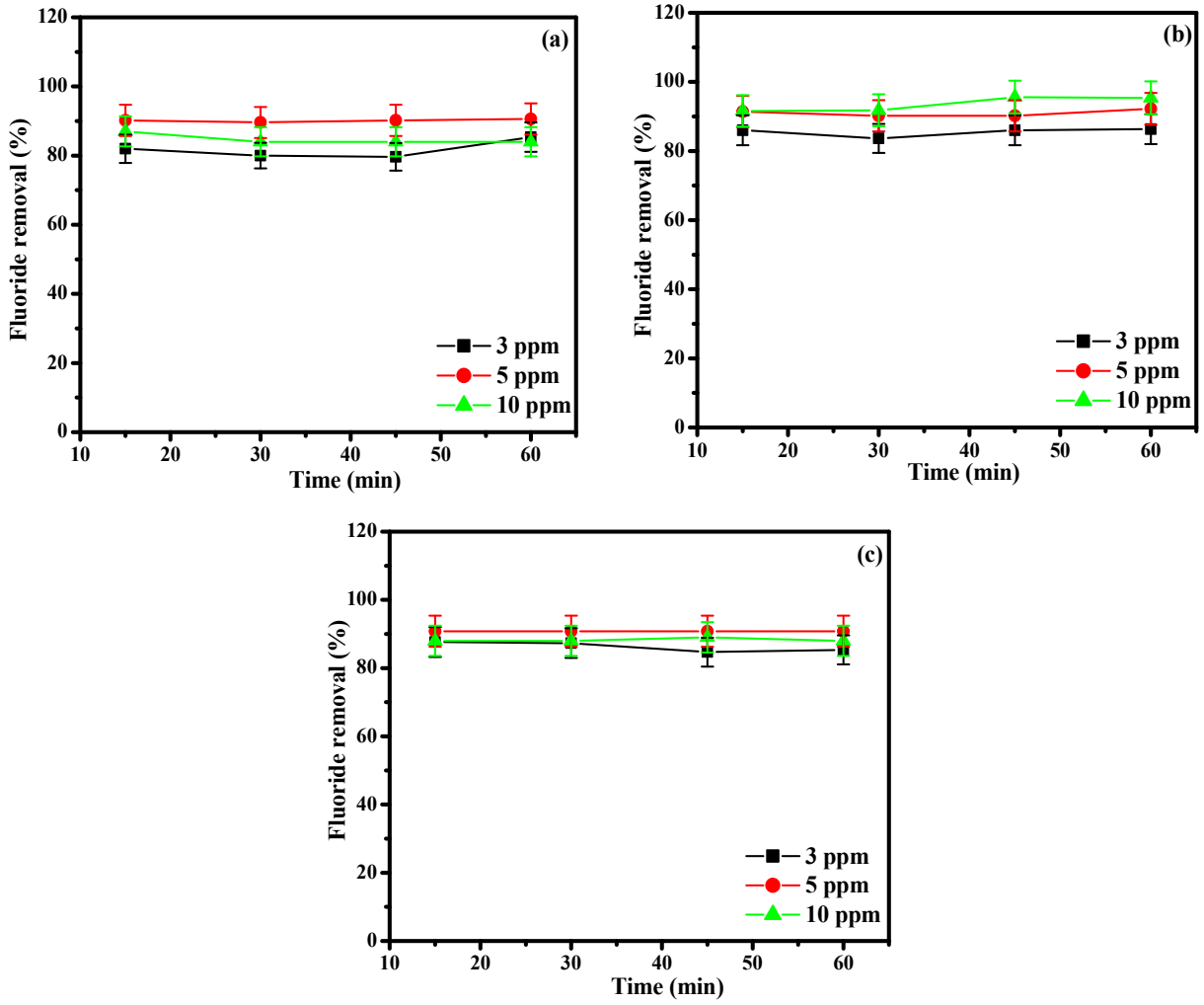

Fig.S8. Fluoride removal vs. contact time taking (a) 0.05 g/100 ml, (b) 0.10 g/100 ml, (c) 0.15 g/100 mL the adsorbent dose of Fe-Al BDC prepared at 473K for 70h.

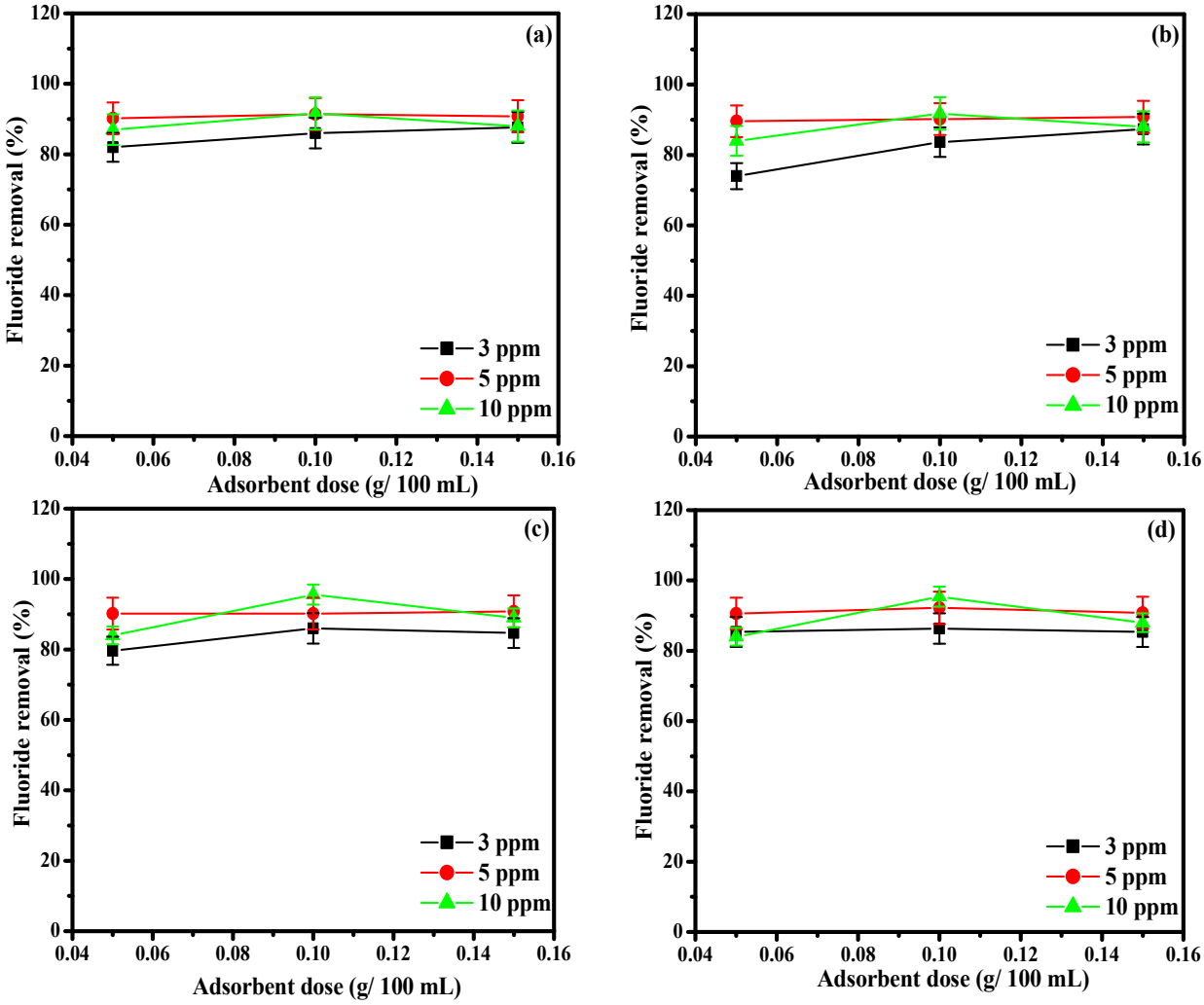

Fig.S9. Fluoride removal vs. adsorbent dose (g/ 100 mL) for (a) 15 min, (b) 30 min, (c) 45 min, and (d) 60 min contact time using Fe-Al BDC prepared at 473K for 70h.

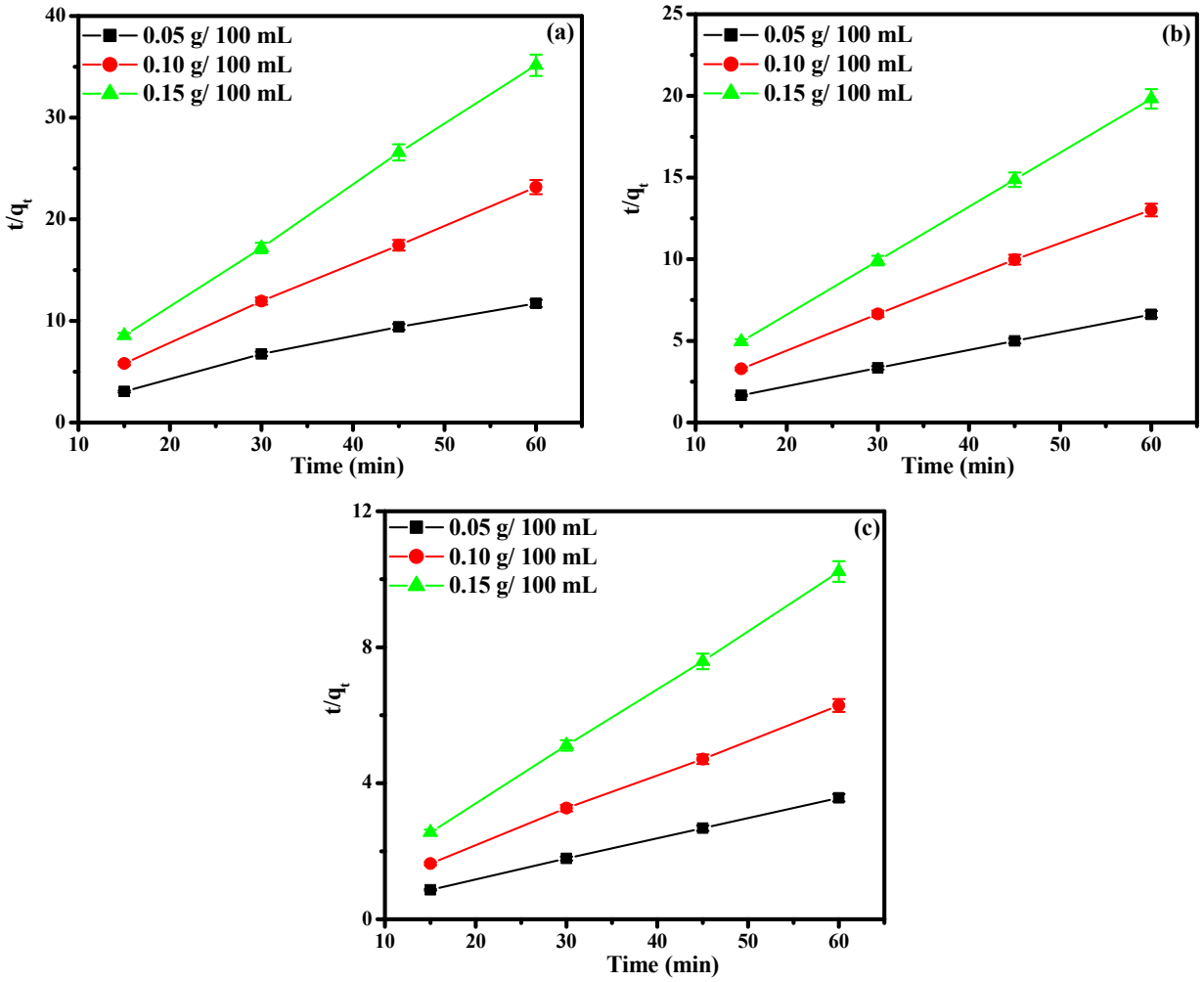

Fig.S10. Pseudo-2nd-order kinetic study using Fe-Al BDC prepared at 473K for 70h with initial fluoride solutions (a) 3 ppm, (b) 5 ppm, (c) 10 ppm.

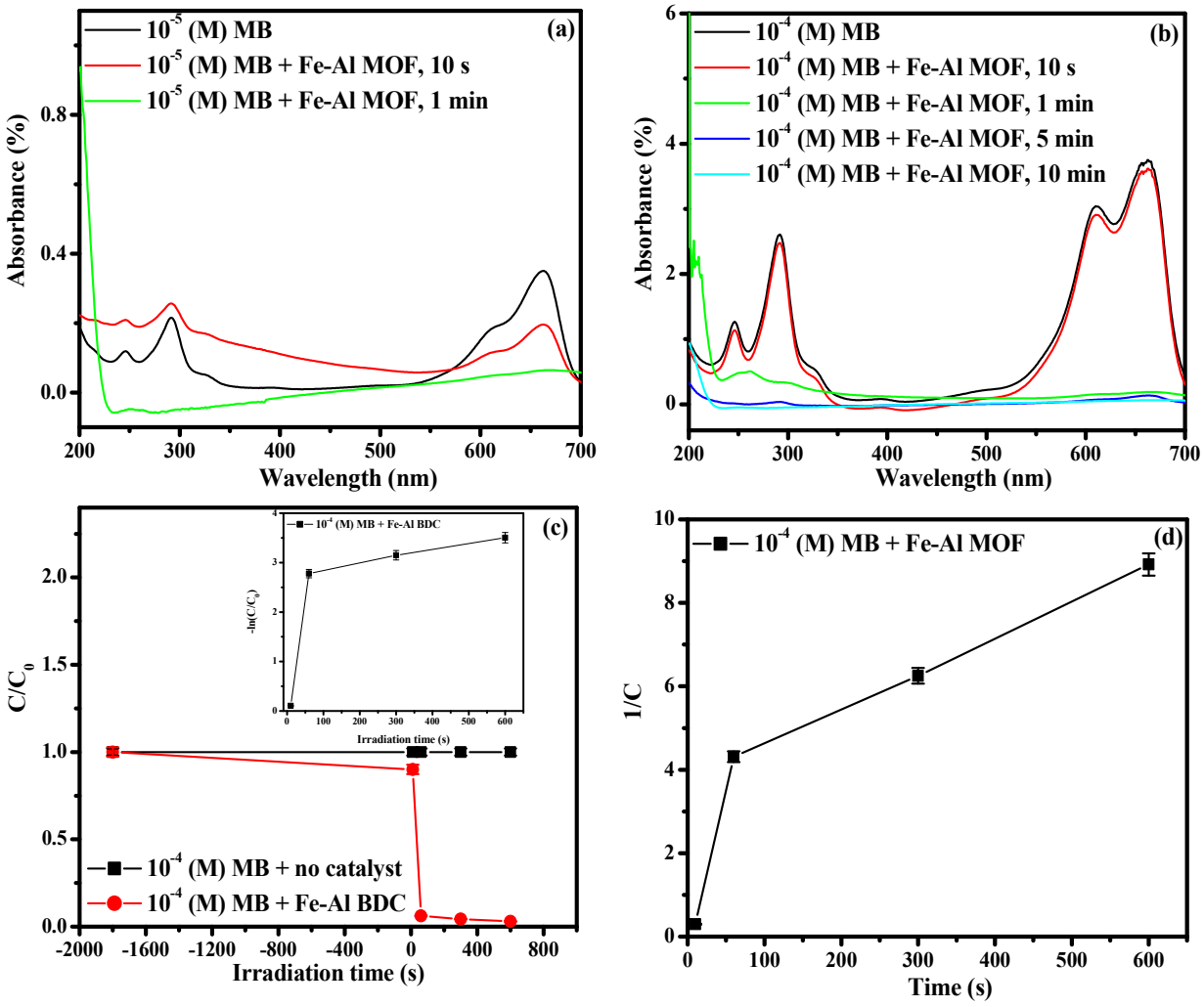

Fig.S11. (a) UV-vis spectral analysis of 10^{-5} (M) and (b) 10^{-4} (M) MB photodegradation, (c) variation of change of concentration with the solar irradiation time (inset-pseudo-1st-order kinetic plot), and (d) pseudo-2nd-order kinetic plot of the photodegradation of 10^{-4} (M) MB using Fe-Al BDC prepared at 473K for 70h.

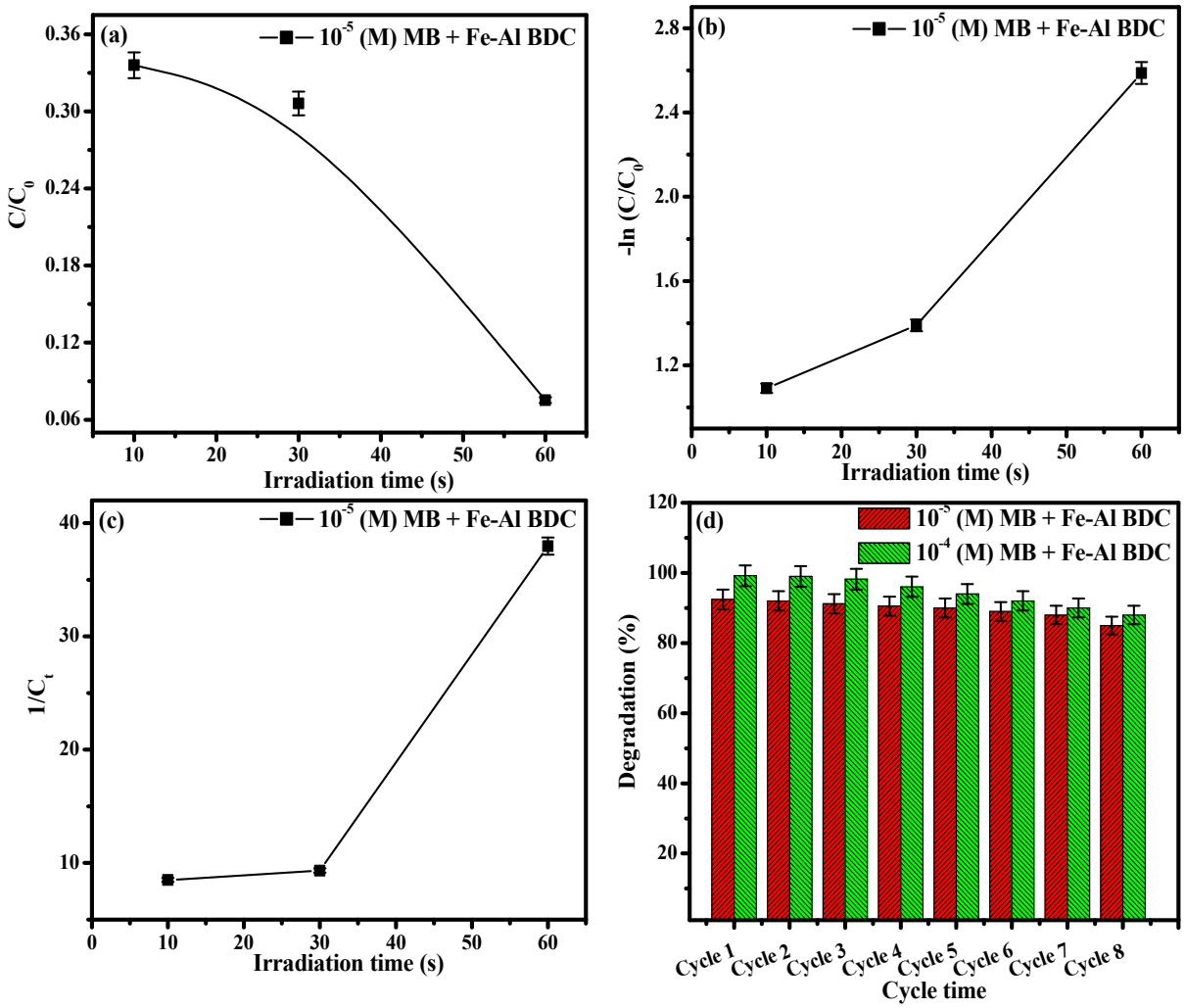

Fig.S12. (a) variation of change of concentration with the solar irradiation time 10^{-5} (M) MB (b) pseudo-1st-order kinetic plot, (c) pseudo-2nd-order kinetic plot, and (d) reuse studies plot of the photodegradation of $10^{-5}/10^{-4}$ (M) MB using 0.10 g/ 100 mL Fe-Al BDC prepared at 473K for 70h.

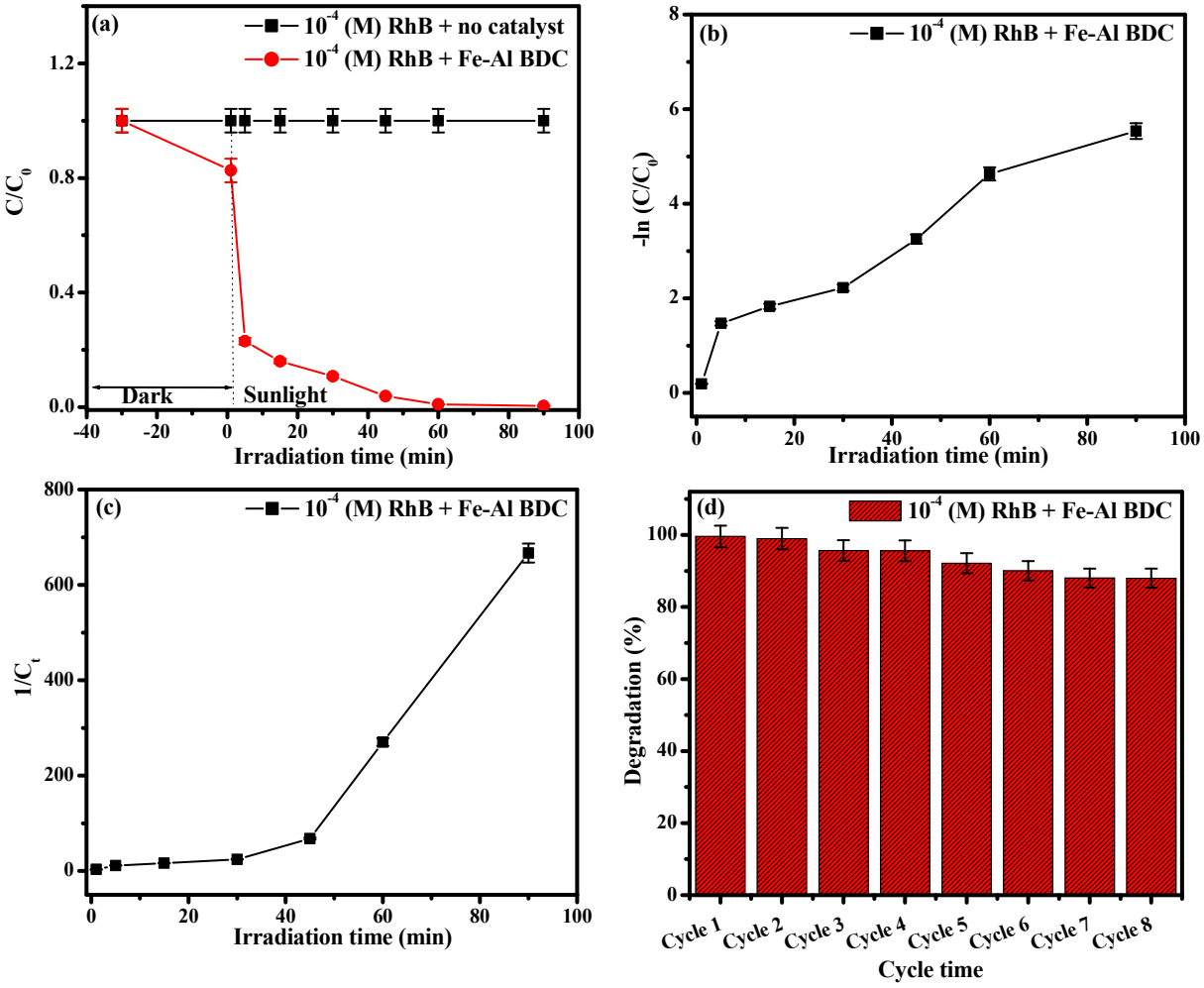

Fig.S13. (a) Variation of Change in concentration with the solar irradiation time (b) pseudo-1st-order kinetic plot, (c) pseudo-2nd-order kinetic plot, and (d) reuse study of the photodegradation of 10^{-4} (M) RhB using 0.10 g/ 100 mL Fe-Al BDC prepared at 473K for 70h.

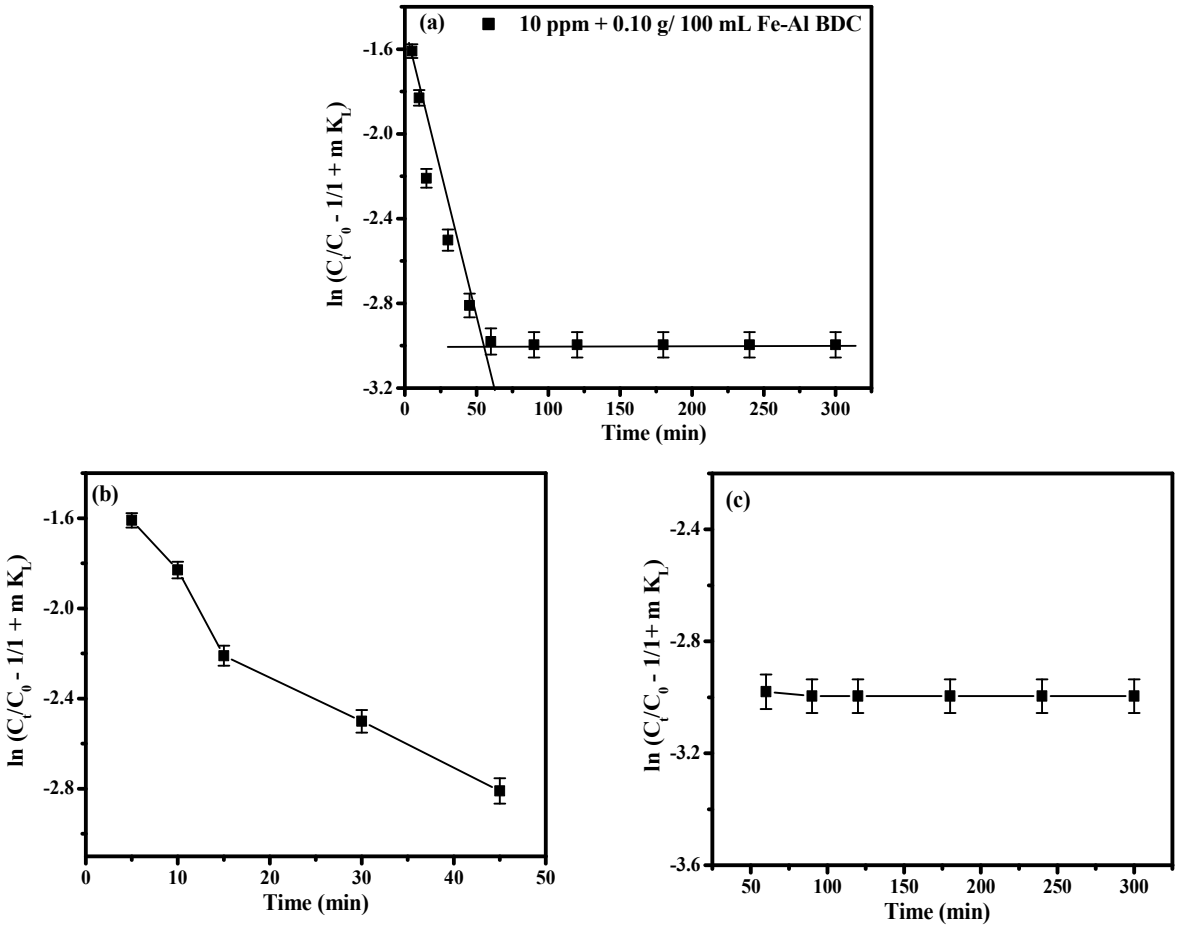

Fig.S14. Mass transfer plot for the adsorption of fluoride onto 0.10 g/ 100 mL Fe-Al BDC prepared at 473K for 70h (a) for 5-300 min, (b) up to 45 min, and (c) up to 300 min.

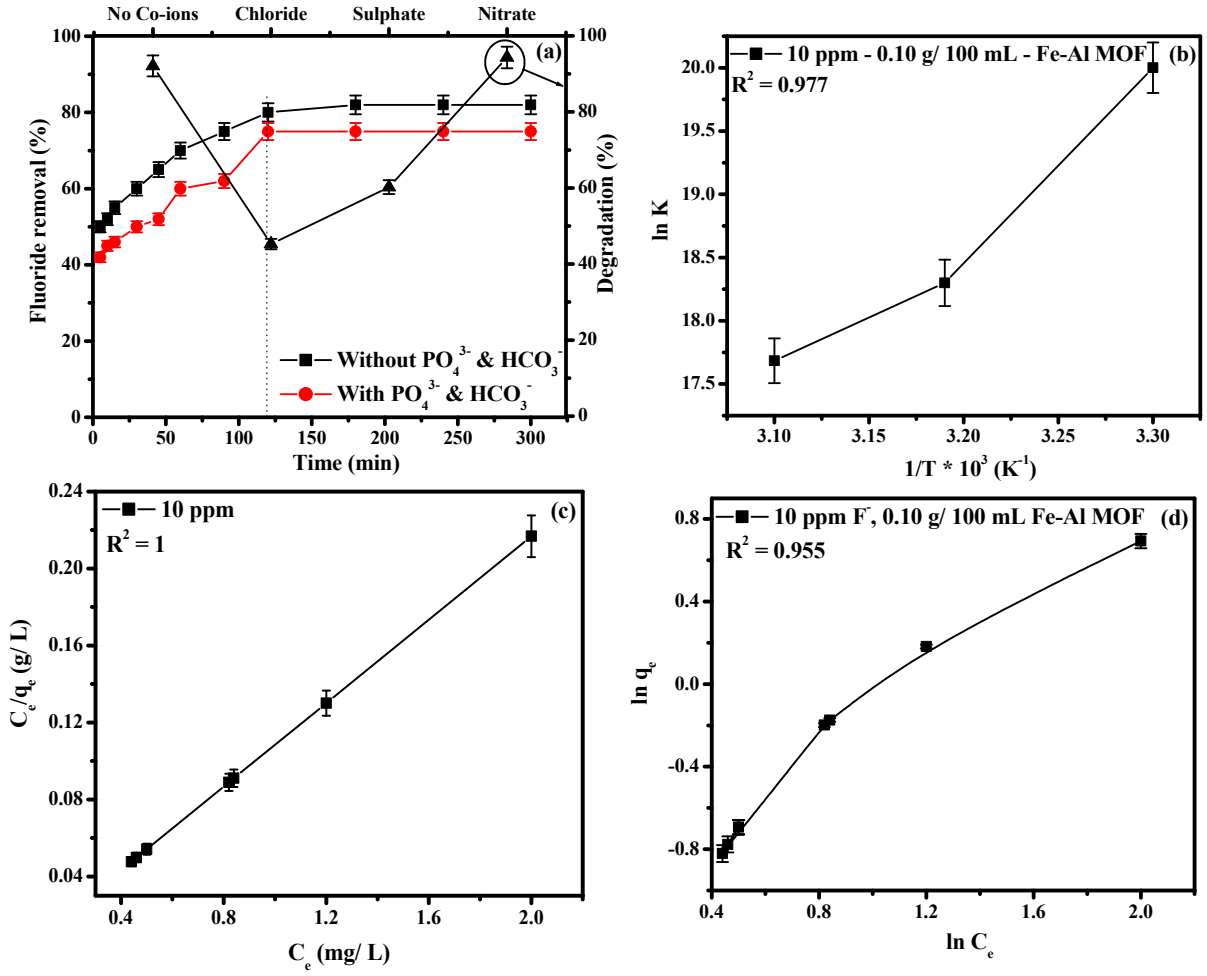

Fig.S15. (a) Effect of co-ions on 10 ppm initial F^- solution and photodegradation of 10^{-5} (M) RhB, (b) thermodynamic studies, (c) Langmuir isotherm, and (d) Freundlich isotherm studies for 10 ppm initial F^- solution using 0.10 g/ 100 mL Fe-Al BDC (F^- adsorption related studies were done at 30°C) prepared at 473K for 70h.

FTIR study of chemisorption of fluoride

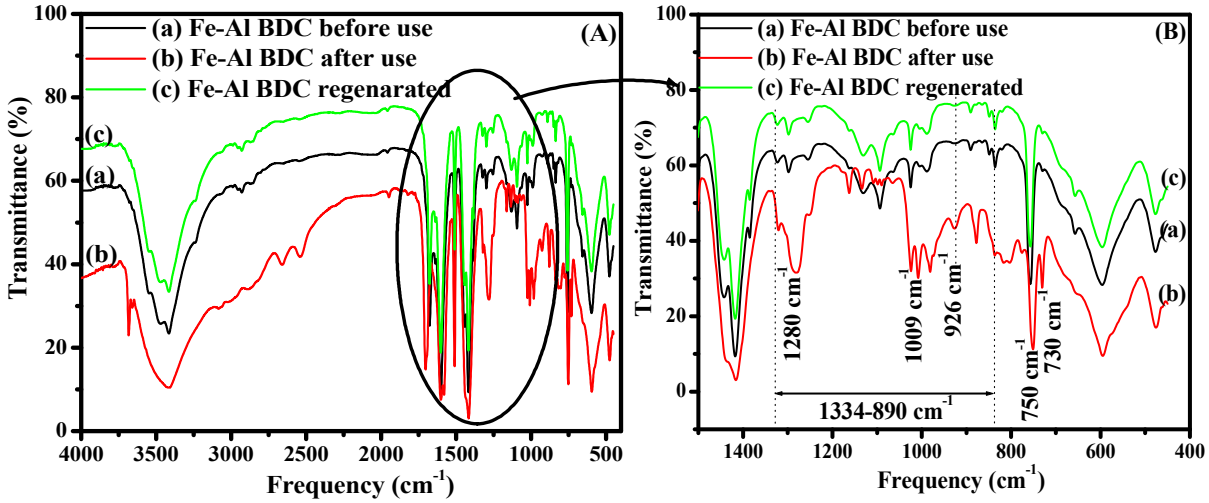

Fig.S16. (A) FTIR studies of Fe-Al BDC: (a) before use, (b) after use (fluoride adsorbed), and (c) regenerated. (B) magnified FTIR studies 1500-400 cm^{-1} of Fe-Al BDC for the fluoride adsorption studies using 0.10 g/100 mL Fe-Al BDC prepared at 473K for 70h.

Fig.S16 shows the FTIR analysis of Fe-Al BDC used for the fluoride removal at pH7. The adsorbents were collected using centrifugation followed by filtration after the batch studies and the regeneration was done using previously reported method [8] and the regenerated FTIR of Fe-Al BDC almost merged with Fe-Al BDC before use, which indicated that the regeneration process was done properly and assured that the adsorbents were fit for batch studies without any adverse effect as shown inFig.S16A(a-c). Fe-Al BDC consists of two trivalent hard-acid centers i.e., Fe^{3+} and Al^{3+} and the hard center F^- prefers to bind with these hard centers present in Fe-Al BDC and a similar thing has been observed in the FTIR analysis of Fe-Al BDC before and after the fluoride adsorption process as shown in Fig.S16A-B. The chemisorption peaks for the fluoride adsorption onto Fe-Al BDC could be visible in Fig.S16B (magnified 1500-400 cm^{-1}) as the peak intensities were majorly changed from 1500-400 cm^{-1} in the fluoride removal experiment. The peaks around 1334-890 cm^{-1} were for the asymmetric Al−O stretching modes [9] and after fluoride adsorption significant Al–F bands were observed at 1280, 1009, and 926 cm^{-1} respectively [10] which also indicates that the adsorption of fluoride onto Fe-Al BDC depended on ion exchange with –OH bound Fe-Al BDC surface [4]. The peaks at 750, and 725 cm^{-1} after the fluoride adsorption indicate

that the formation of Fe—F bond, probably the formation of FeF_4 [11] species as shown in Fig.S16B-b.

FTIR study of photodegradation of RhB

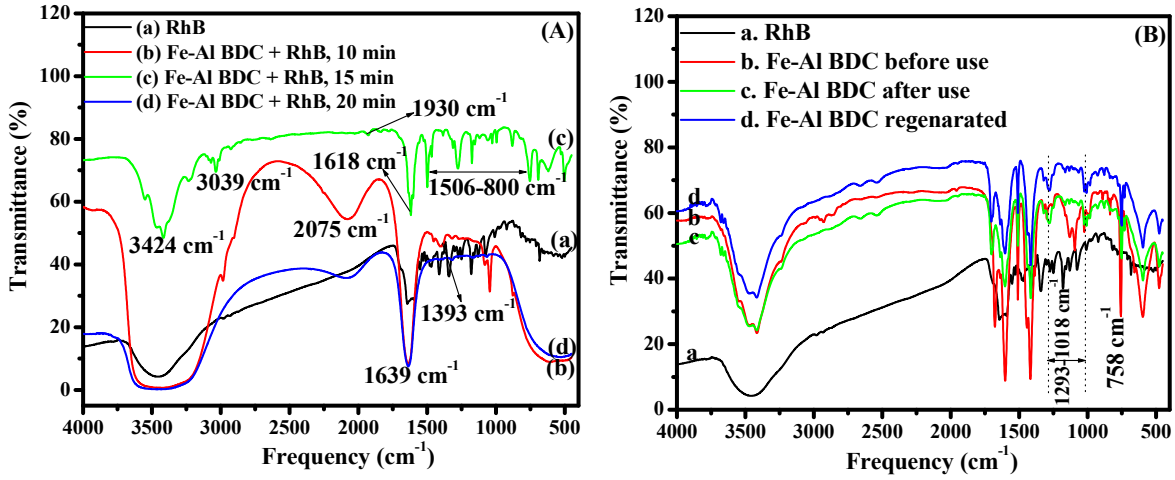

Fig.S17. (A) FTIR studies of different aliquots of the photodegradation of 10^{-5} (M) RhB using 0.10g/ 100 mL Fe-Al BDC: (a) RhB, (b) 10 min aliquot, (c) 15 min aliquot and (d) 20 min aliquot. (B) Fe-Al BDC used in the photodegradation of 10^{-5} (M) RhB (a) RhB, (b) Fe-Al BDC before use, (c) Fe-Al BDC after use, and (d) Fe-Al BDC regenerated prepared at 473K for 70h.

Fig.S17 A and B represent the FTIR analysis of different aliquots taken in the different time intervals in the photodegradation of 10^{-5} (M) RhB using 0.10 g/ 100 mL Fe-Al BDC and the FTIR of Fe-Al BDC used in this photodegradation process respectively. In Fig.S17A, a strong stretching frequency at 3500 cm^{-1} and 1640 cm^{-1} were observed for RhB indicating the presence —COOH and —N–H stretching of NH_2 (primary amine) group respectively [12]. In Fig.S17A it could be noticed that the characteristic peaks of RhB gradually disappeared with the prolonged solar irradiation time or the photodegradation reaction time. For 10 min aliquot the presence of 1393, 1639, 2075 cm^{-1} bands describe the stretching modes of —NH_2 [9] which were formed through the de-ethylation step as described in the mechanism section of the manuscript. For 15 min aliquot, the peaks at 3424-3039 cm^{-1} are attributed to N–H stretching, 1930 cm^{-1} is due to asymmetric C–H and symmetric C–H stretching vibrations [13] and 1618 cm^{-1} represents the existence of benzenoid ring and C=N stretching mode for imine respectively. The peak at 1560

cm^{-1} represents the vibration of N–H and peaks from 1506-800 cm^{-1} are related to C=C stretching vibration, C–N stretching mode, and the peak at 800 cm^{-1} is assigned to the plane bending vibration of C–H of for benzenoid ring [14]. Thus, from the FTIR analysis, it could be said that aniline is formed in this step which was also supported by the HPLC study as stated in the mechanism section of the manuscript. For the 20 min aliquot there is no characteristic peaks around 1500-400 cm^{-1} indicating the complete disappearance of the aromatic structure of RhB which leads to mineralization of the dye moiety in this photodegradation process as shown in Fig.S17A.

In Fig.S17B the FTIR spectra of Fe-Al BDC during the photodegradation process have been recorded and compared with the FTIR of RhB. In the collected FTIR spectrum of Fe-Al BDC i.e., after use (Fig.S17B-c) bands observed at 1293-1018 cm^{-1} and shortening of the band at 758 cm^{-1} was due to the formation of the metal-nitrogen bond [15] which could be due to the adsorption of aniline over the Fe-Al BDC surface which is shown in the mechanism section of the manuscript. This adsorption of aniline onto Fe-Al BDC surface occurred as the pK_a of aniline i.e., 4.6. As the pH_{ZPC} of Fe-Al BDC is 7.22 and thus, the adsorption of aniline occurred onto Fe-Al BDC positively charged surface.

Table S4. Physical parameters of the different concentrations RhB solutions and 0.01 (M) Na-salts dissolved in 10^{-5} (M) RhB solution at 30°C.

Serial no.	pH		Conductance (μScm^{-1})		Salinity (psu)		Resistivity ($\kappa\Omega cm$)		TDS (ppm)	
	Initial	Final	Initial	Final	Initial	Final	Initial	Final	Initial	Final
10^{-5} (M)	5.62	9.08	30.69	24.58	0.023	0.019	32.43	50.26	15.08	6.99
10^{-4} (M)	4.34	10.62	24.66	14.61	0.021	0.017	43.11	67.70	11.95	7.12
10^{-5} (M) + 0.01 (M) NaCl	5.30	8.95	1473	1450	0.740	0.623	679.40	695.81	7.220	6.326
10^{-5} (M) + 0.01 (M) Na_2SO_4	5.24	8.92	2722	2690	1.416	0.899	364.60	370.23	1.337	0.994

10^{-5} (M) + 0.01 (M) $NaNO_3$	5.23	8.90	1450	1360	0.726	0.654	691.30	695.49	7.099	6.055
10^{-5} (M) + 0.01 (M) Na_3PO_4	11.47	11.85	2007	1989	1.025	0.987	496.80	498.90	9.852	8.012

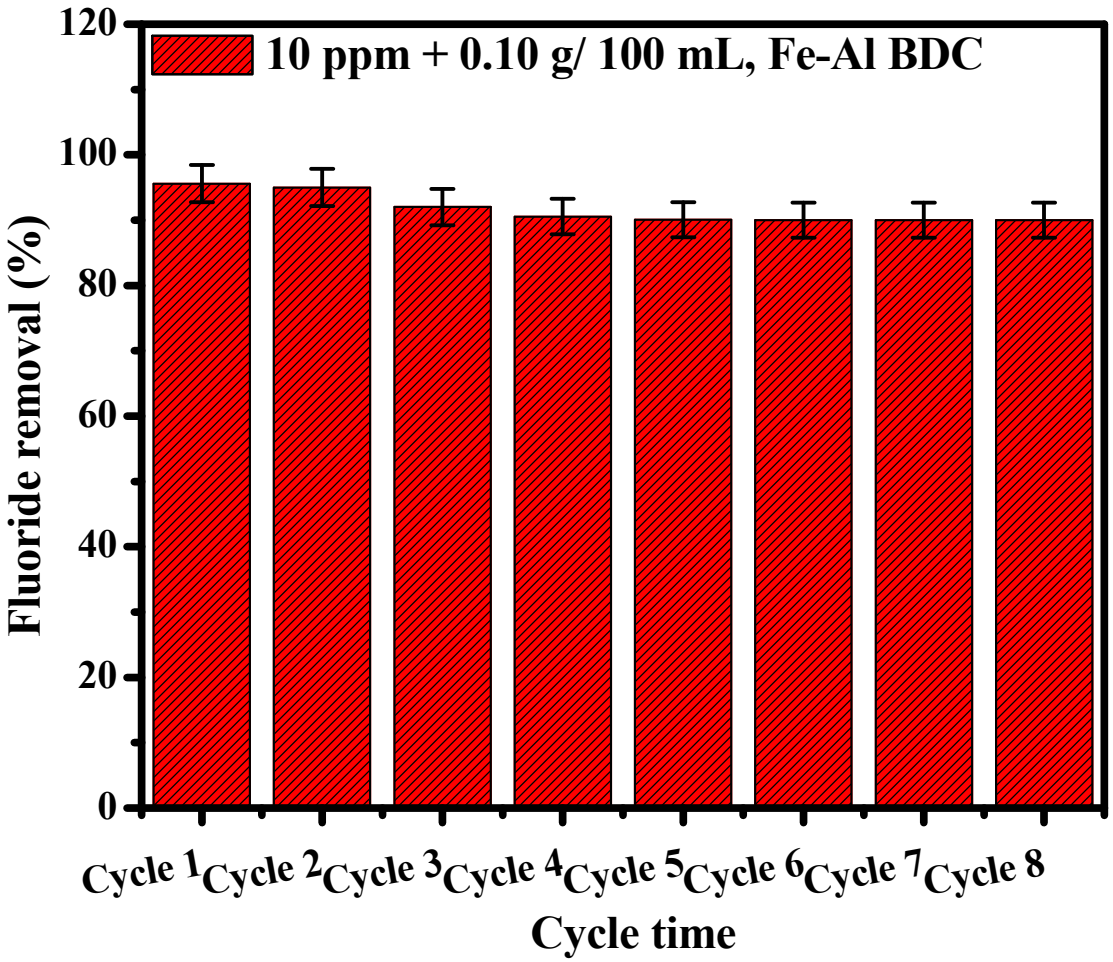

Fig.S18. Reuse study for fluoride adsorption using 0.10 g/ 100 mL Fe-Al BDC prepared at 473K for 70h.

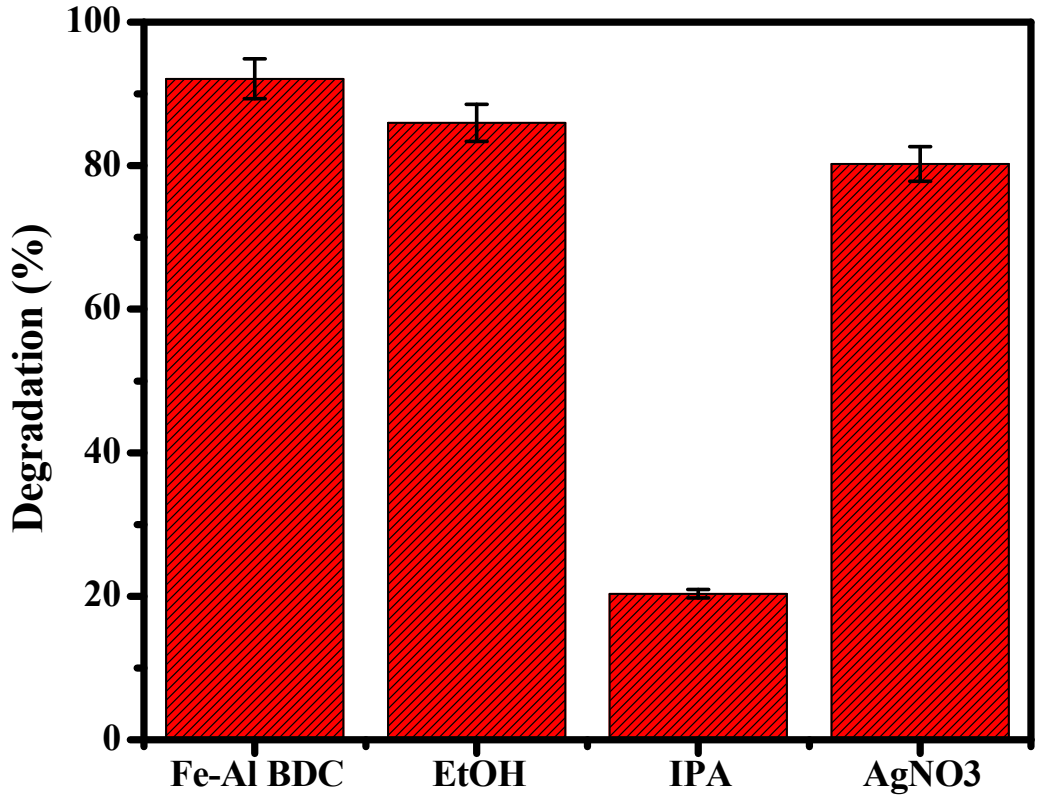

Fig.S19. Photocatalytic degradation of 10^{-5} (M) RhB using 0.10 g/ 100 mL Fe-Al BDC prepared at 473K for 70h in different scavengers under Sunlight irradiation.

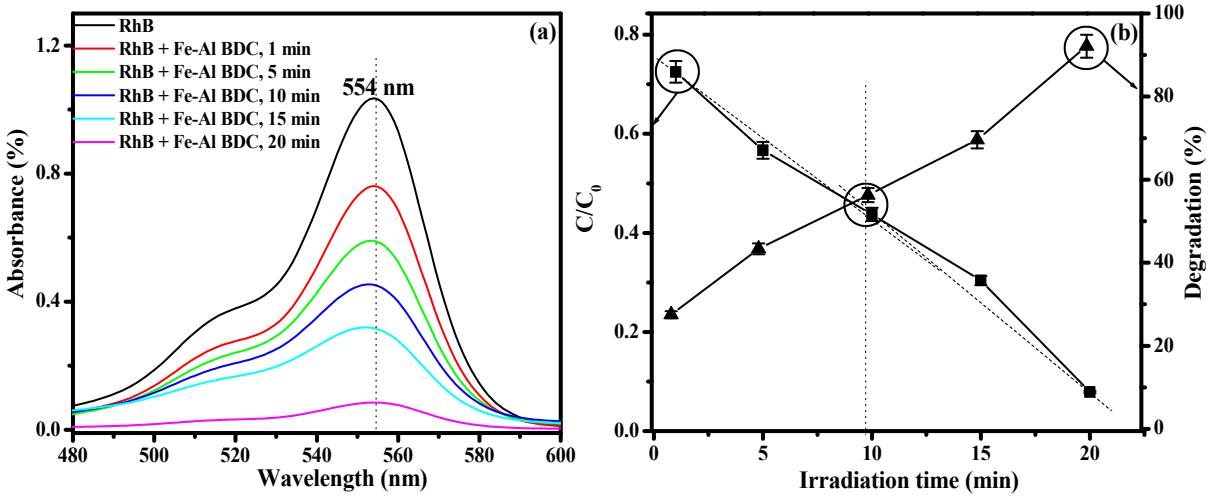

Fig.S20. (a) UV-vis spectral analysis of the photodegradation showing the hypochromic shift (partly enlarged) and (b) change in concentration with the % degradation and two-step kinetic model of 10^{-5} (M) RhB using 0.10 g/100 mL Fe-Al BDC prepared at 473K for 70h.

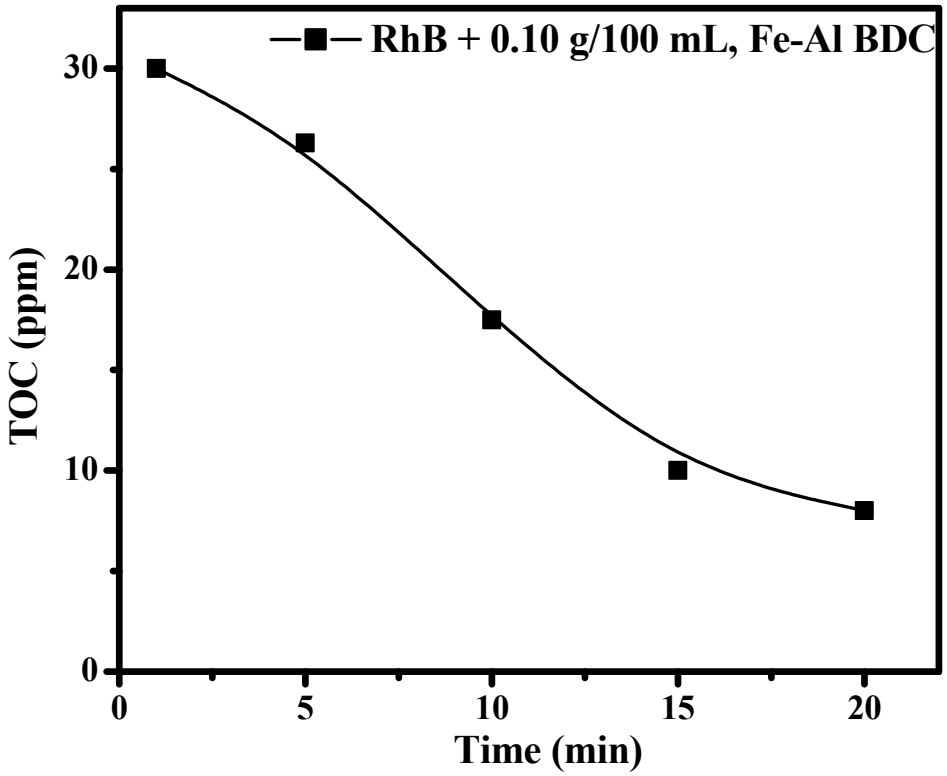

Fig.S21. TOC disappearance of photodegradation of 10^{-5} (M) RhB using 0.10 g/ 100 mL Fe-Al BDC prepared at 473K for 70h.

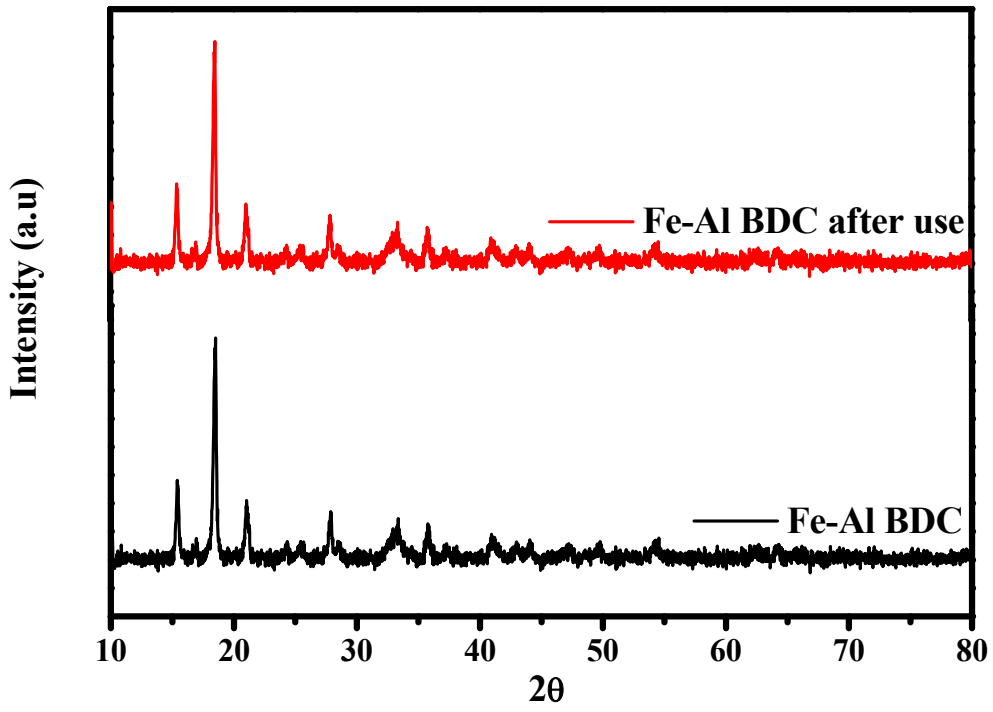

Fig.S22. PXRD analysis of Fe-Al BDC prepared at 473K for 70h before and after use (regenerated) of the photodegradation of RhB under solar irradiation.

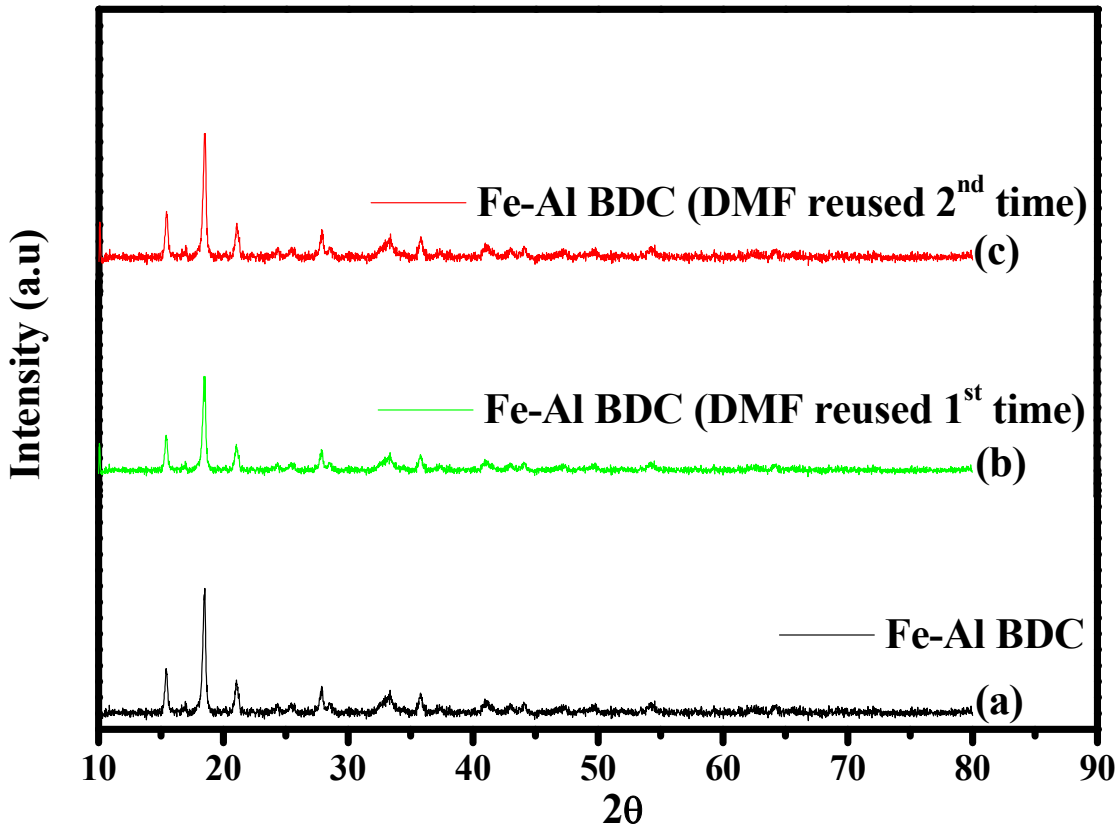

Fig.S23. PXRD analysis (a) Fe-Al BDC, (b) Fe-Al BDC prepared from the collected DMF used in the 1st synthesis, (c) Fe-Al BDC prepared from the DMF used in the 2nd synthesis prepared at 473K for 70h.

Table S5. Determination of F^{-}, Cl^{-}, NO_3^{-}, SO_4^{2-}, PO_4^{3-}, and HCO_3^{-} ion concentrations in the prepared samples (L1, L2) and various field samples (F1, F2, F3, F4) collected from the 10 km belt of latitude and longitude of 23.3613° N, 86.3399° E respectively.

Name	F^{-}		Cl^{-}		NO_3^{-}		SO_4^{2-}		PO_4^{3-}		HCO_3^{-}	
	Initial	Final	Initial	Final	Initial	Final	Initial	Final	Initial	Final	Initial	Final
L1	10	0.90	500	230	50	30	500	270	-	-	-	-
L2	10	1.20	500	242	50	35	500	232	500	224	250	140
F1	1.90	0.08	152.02	76.09	25.66	8.56	40.23	22.36	80.59	45.06	202	89
F2	1.80	0.07	150.23	74.11	25.06	8.52	44.22	25.01	78.99	43.54	200	89
F3	0.66	0.02	160	75.89	20.56	6.64	50.26	26.12	85.28	47.01	240	104
F4	0.26	0.01	162	78.54	21.62	6.68	52.66	22.55	70.11	39.05	223	98

Reference

1. Sana Khan, A.M., *Environmental and Health Effects of Textile Industry Wastewater.* Environmental Deterioration and Human Health, 2013: p. 55-71.
2. M. Ali, T.R.S., *Aquatic Toxicity from Pulp and Paper Mill Effluents: A Review.* Adv. Environ. Res., 2001. **5**(2): p. 175-196.
3. Sankha karmakar, J.D., Christoph Janiak, Sirshendu De, , *Aluminium fumarate metal-organic framework: A super adsorbent for fluoride from water, .* Journal of Hazardous Materials 2016. **303**: p. 10-20.
4. Nantong Zhang, X.Y., Xinyao Yu, Yong Jia, Jin Wang, Lingtao Kong,Zhen Jin, Bai Sun, Tao Luo, Jinhuai Liu, *Al-1,3,5-benzenetricarboxylic metal-organic frameworks: A promising adsorbent for defluoridation of water with pH insensitivity and low aluminum residual.* Chemical Engineering Journal, 2014. **252**: p. 220–229.
5. Anirban Chowdhury, M.K.A., Arnab Mukherjee, Prasanta Dhak, Julekha Khatun, Debasis Dhak, *A critical review on geochemical and geological aspects of fluoride belts, fluorosis and natural materials and other sources for alternatives to fluoride exposure.* Journal of Hydrology, 2019. **574**: p. 333–359.
6. M. Vithanage, P.B., *Fluoride in the environment: sources, distribution and defluoridation.* Environ. Chem. Lett., 2015. **13**(2): p. 131–147.
7. M. André, M.E.M., I. Neretnieks, *Specific surface area determinations on intact drillcores and evaluation of extrapolation methods for rock matrix surfaces.* Journal of Contaminant Hydrology, 2009. **110**: p. 1-8.
8. M. K. Adak, A.S., A. Mukherjee, S. Sen, D. Dhak, *Removal of fluoride from drinking water using highly efficient nano-adsorbent, Al(III)-Fe(III)-La(III) trimetallic oxide prepared by chemical route.* J. Alloys Compd, 2017. **719**: p. 460−469.
9. A. Mukherjee, M.K.A., A. Chowdhury, D. Dhak, *Synthesis of Cost-effective Trimetallic Oxide Nanocatalysts for the Reduction of Nitroarenes in Presence of $NaBH_4$ in an Aqueous Medium.* Current Catalysis, 2019. **8**: p. 41-55.
10. Arnab Mukherjee, A.C., Mrinal K. Adak, Julekha Khatun, Prasanta Dhak, Debasis Dhak, *Fluoride adsorption and photoreduction of Cr(VI) using heterogeneous Al^{3+} modified mine-waste, an in-situ approach.* Journal of Environmental Chemical Engineering, 2020. **8**: p. 103759.
11. Alexandre Vimont, J.-C.L., Loic Francke, Alain Demourgues, Alain Tressaud, Marco Daturi, *Infrared Study of the Surface Properties of HTB-Type Al-, Cr-, Fe-Hydroxyfluorides.* J. Phys. Chem. B, 2004. **108**: p. 3246-3255.
12. Malingappa Pandurangappa, K.S.K., *Micellar mediated trace level mercury quantification through the rhodamine B hydrazide spirolactam ring opening process.* Anal. Methods., 2011. **3**: p. 715–723.
13. J. Vivekanandan, V.P., A. Mahudeswaran, P. S. Vijayanand, *Synthesis, characterization and conductivity study of polyaniline prepared by chemical oxidative and electrochemical methods.* Archives of Applied Science Research, 2011. **6**: p. 147–153.

14. He, Y., *A novel emulsion route to sub-micrometer polyaniline/nano-ZnO composite fbers.* Applied Surface Science, 2005. **249**: p. 1-6.
15. S. A. Rounaghi, H.E., S. Scudino, A. Vyalikh, D. E. P. Vanpoucke, W. Gruner, S. Oswald, A. R. Kiani Rashid, M. Samadi Khoshkhoo, U. Scheler, J. Eckert, *Mechanochemical route to the synthesis of nanostructured Aluminium nitride.* Scientific Reports, 2016. **6**.